inorganics

MDPI

Article

A Heterobimetallic Au(I)–Ru(II) Complex Bridged by dppb: Synthesis, Structural and Solution Characterization, BSA Interaction and In Vivo Toxicity Evaluation in Wistar Rats †

Adnan Zahirović [1,*], Sunčica Roca [2], Muhamed Fočak [3], Selma Fetahović [1], Višnja Muzika [4], Damir Suljević [3], Anela Topčagić [1], Maja Mitrašinović-Brulić [3], Irnesa Osmanković [1], Debbie C. Crans [5] and Aleksandar Višnjevac [2,*]

[1] Laboratory for Inorganic and Bioinorganic Chemistry, Department of Chemistry, Faculty of Science, University of Sarajevo, 71000 Sarajevo, Bosnia and Herzegovina
[2] Ruđer Bošković Institute, 10000 Zagreb, Croatia
[3] Department of Biology, Faculty of Science, University of Sarajevo, 71000 Sarajevo, Bosnia and Herzegovina
[4] Department of Histology and Embryology, Faculty of Medicine, University of Sarajevo, 71000 Sarajevo, Bosnia and Herzegovina
[5] Department of Chemistry and Cell & Molecular Biology Program, Colorado State University, Fort Collins, CO 80523, USA
* Correspondence: adnan.zahirovic@pmf.unsa.ba (A.Z.); aleksandar.visnjevac@irb.hr (A.V.); Tel.: +387-33-279-917 (A.Z.); +385-14-571-203 (A.V.)

† Zahirović, A.; Roca, S.; Fočak, M.; Fetahović, S.; Višnjevac, A.; Topčagić, A.; Suljević, D.; Mitrašinović-Brulić, M.; Ostojić, J.; Muzika, V. Heterobinuclearity vs. Homobinuclearity in Ruthenium (II) and Gold (I) Organometallics with Diphosphine Ligands: Synthesis, Characterization, BSA Binding, and In Vivo Toxicity. In Proceedings of the 5th International Congress of Chemists and Chemical Engineers of Bosnia and Herzegovina, Sarajevo, Bosnia and Herzegovina, 27–30 June 2024; Book of Abstracts; p. 128.

Abstract

A novel heterobimetallic ruthenium(II)–gold(I) complex featuring a bridging bis(diphenylphosphino)butane (dppb) ligand was prepared and fully characterized. Single-crystal X-ray diffraction revealed a piano-stool geometry around Ru(II) with η^6-cymene, two chlorido ligands, and one phosphorus atom from dppb, while the Au(I) center adopts a linear P–Au–Cl coordination. Structural integrity in the solution was confirmed by 1D and 2D NMR spectroscopy, while solution behavior was further monitored by variable solvent ^{31}P NMR and UV/Vis spectroscopy, indicating that the organometallic Ru–arene core remains intact, whereas the chlorido ligands coordinated to Ru exhibit partial lability. Complementary characterization included elemental analysis, FTIR, and UV/Vis spectroscopy. Spectrofluorimetric and FRET analyses showed that Au(dppb), Ru(dppb), and the heterobimetallic AuRu complex bind to BSA with apparent constants of 1.41×10^5, 5.12×10^2, and 2.66×10^4 M^{-1}, respectively, following a static quenching mechanism. In vivo biological evaluation in Wistar rats revealed no significant hepatotoxicity or nephrotoxicity, with only mild and reversible histological alterations and preserved hepatocyte nuclear morphology. Hematological analysis indicated a statistically significant reduction in leukocyte populations, suggesting immunomodulatory potential, while elevated serum glucose levels point to possible endocrine or metabolic activity. These findings highlight compound structural stability and intriguing bioactivity profile, making it a promising platform for further organometallic drug development and testing.

Keywords: heterobimetallic complex; ruthenium(II)–gold(I); bis(diphenylphosphino)butane (dppb); Wistar rats in vivo toxicity; immunomodulatory potential

check for updates

Academic Editor: Philippe Schollhammer

Received: 2 September 2025
Revised: 18 September 2025
Accepted: 25 September 2025
Published: 29 September 2025

Citation: Zahirović, A.; Roca, S.; Fočak, M.; Fetahović, S.; Muzika, V.; Suljević, D.; Topčagić, A.; Mitrašinović-Brulić, M.; Osmanković, I.; Crans, D.C.; et al. A Heterobimetallic Au(I)–Ru(II) Complex Bridged by dppb: Synthesis, Structural and Solution Characterization, BSA Interaction and In Vivo Toxicity Evaluation in Wistar Rats. *Inorganics* **2025**, *13*, 323. https://doi.org/10.3390/inorganics13100323

Copyright: © 2025 by the authors. Licensee MDPI, Basel, Switzerland. This article is an open access article distributed under the terms and conditions of the Creative Commons Attribution (CC BY) license (https://creativecommons.org/licenses/by/4.0/).

1. Introduction

Since Rosenberg's pioneering discovery of the antitumor activity of cisplatin and the subsequent opening of the field of metal-based drugs, numerous strategies have been employed to improve their therapeutic profile by enhancing biological activity, reducing toxicity, and increasing selectivity. Despite the diversity of approaches, all of them ultimately rely on a precise definition of the structural elements that govern the activity of coordination compounds and determine their interaction with biological targets. A relatively recent and conceptually powerful strategy in this field is the use of heterobimetallic complexes, in which two distinct metal centers cooperate within a single molecular framework [1]. Such complexes can achieve synergistic effects that go beyond the capabilities of monometallic analogues. Within this context, the "bait-and-drug" design has emerged as a particularly attractive paradigm, where one metal center ensures recognition or delivery, while the other contributes to the biological or catalytic activity. Such dual functionality broadens the chemical space of potential drug candidates and offers new opportunities for fine-tuning structure–activity relationships in medicinal inorganic chemistry [2,3]. However, the synthetic challenges associated with the preparation of such heterobimetallic architectures remain considerable. Issues such as controlling metal–metal distances, ensuring selective coordination modes, and maintaining stability under physiological conditions often complicate their design and reproducibility. Thus, this area is still far less mature and less fruitful compared to the development of monometallic drug candidates, which has already produced several clinically approved compounds and a large body of structure–activity data. Nevertheless, the potential advantages of heterobimetallic complexes, particularly their capacity to integrate synergistic interactions and to exploit novel modes of biological activity, continue to motivate sustained research efforts aimed at overcoming these obstacles and expanding the scope of medicinal inorganic chemistry.

Among transition-metal-based anticancer agents, water-soluble arene ruthenium complexes have emerged as desirable candidates, not only owing to the presumed affinity of cancer cells for ruthenium as an iron congener [4] and the low systemic toxicity displayed by numerous ruthenium derivatives [5], but also because these organometallic scaffolds uniquely combine hydrophilic and lipophilic characteristics, which are essential for their efficient transport and distribution in biological environments [6,7]. A notable representatives of this class are complexes (η^6-*p*-MeC_6H_4Pri)Ru(PTA)Cl_2 (PTA = 1,3,5-triaza-7-phosphaadamantane), commonly referred to as RAPTA-C [8] and its structural variations [9–11], a variety of mononuclear arene ruthenium complexes containing N-donor imidazole-based ligands [12], cationic arene ruthenium complexes incorporating ethylenediamine (en) chelating ligands, along with structurally related analogues [13]. Beyond these examples, numerous arene ruthenium complexes with NN, NO, and OO donor ligands have also been synthesized and evaluated for their biological potential [13–15].

In parallel, gold(I) complexes have been extensively explored as selective and potentially less toxic antitumor agents [16], exerting their biological activity primarily through inhibition of thiol- and selenol-containing enzymes, thereby disrupting redox homeostasis in malignant cells, particularly those resistant to conventional therapies [17]. Gold(I) species coordinated with phosphines [18], N-heterocyclic carbenes (NHCs) [19,20], thiolates [21,22], alkynyl groups [23,24], thioureas [25], triazole–peptides [26], and related ligands have been shown to potently inhibit thiol-containing enzymes such as thioredoxin reductase (TrxR), with inhibitory effects observed at nanomolar concentrations. For example, the clinically used antiarthritic drug auranofin has exhibited pronounced in vitro cytotoxicity against a wide spectrum of human cancer cell lines, along with proven efficacy in vivo in the P388 leukemia mouse model [27].

Several heterobinuclear ruthenium–gold complexes have been described in the literature, exemplified by the combination of RAPTA-derived ruthenium fragments [28] with an auranofin-based gold fragment [29] to yield [(η^6-*p*-cymene)$RuCl_2$(μ-dppm)Au(IMes)]ClO_4 (RANCE-1), where dppm = bis(diphenylphosphino)methane and IMes = 1,3-bis(2,4,6-trimethylphenyl)imidazol-2-ylidene. This compound was about three times less cytotoxic toward human ovarian carcinoma (A2780) cells compared to auranofin [30], while retaining the ability to inhibit thioredoxin reductase, pan-matrix metalloproteinases, pan-cathepsins, and vascular endothelial growth factor [31]. Other related complexes, including [(η^6-*p*-cymene)$RuCl_2$(μ-dppm)AuCl] and [(η^6-*p*-cymene)$RuCl_2$(μ-dppm)Au(S-thiazoline)], have demonstrated comparable antiproliferative profiles irrespective of the identity of the terminal ligand at the gold(I) center [2]. Both displayed superior activity relative to the parent binuclear ruthenium complex [Ru(*p*-cymene)Cl(μ-Cl)]$_2$ and the mononuclear ruthenium analogue [Ru(*p*-cymene)Cl_2(η^1-dppm)], underscoring the significant role played by the covalent incorporation of the gold center into the ruthenium-based molecular scaffold in enhancing biological performance. The introduction of NHC ligands to the gold center in analogous cationic ruthenium(II)–gold(I) architectures has been reported to improve tumor cell selectivity [32]. Inspired by the preferential nucleosome core particle binding of RAPTA-T and auranofin, a series of heterometallic ruthenium(II)–gold(I) complexes was synthesized with variable linker lengths (4–8 PEG units) to systematically assess the effect of linker length on cytotoxic potency [33].

Here, a heterobinuclear complex in which gold(I) and ruthenium(II) centers are bridged through a 1,4-bis(diphenylphosphino)butane ligand is reported [34]. Structural elucidation by single-crystal X-ray diffraction, complemented by a suite of spectroscopic techniques, confirmed the coexistence of both metallic centers within a single molecular framework. The binding affinity of the complex to bovine serum albumin (BSA) and its solution behavior were evaluated to gain insight into its potential bioavailability, stability, and protein interaction profile under physiologically relevant conditions. Furthermore, comprehensive biochemical, hematological, and histological analyses were conducted in vivo in a Wistar rat model to assess the safety profile, toxicity, and potential biomedical applicability.

2. Results and Discussion

2.1. Design and Syntheses

The design of this heterobimetallic assembly stems from the idea of pairing the pharmacophoric Ru(II)–arene "piano-stool" fragment with a soft, thiophilic Au(I) center through a single bridging phosphine, thereby achieving spatial control, potential cooperativity, and modulation of reactivity/bioactivity that cannot be readily accessed by monometallic analogues. In the literature, Ru–Au systems that were consistently reported involve dppm-bridged species of the type [(arene)$RuCl_2$(μ-dppm)AuL], including derivatives inspired by auranofin, in which stable structures and relevant bioactivities have been confirmed, while purely phosphine-bridged scaffolds show limited electronic communication between the metals [2,33,35]. In contrast, examples of Ru–Au complexes bridged by longer chain diphosphines have not been described to the best of our knowledge. Consistent with general chelate stability trends [36,37], dppe and dppp preferentially chelate Ru(II), forming favorable five- and six-membered rings; accordingly, under our experimental conditions, they afforded exclusively mononuclear ruthenium complexes with bidentate phosphine coordination, rather than Ru–Au bridged species. On the other hand, dppb, yielding a potential seven-membered chelate at Ru(II), is less favorable and sterically more demanding, which suppresses intramolecular chelation and enables bridging, thereby stabilizing the Ru(II)–μ-dppb–Au(I) framework.

The heterobimetallic complex [(cym)Cl_2Ru–μ-dppb–AuCl] (AuRu) was obtained by reacting [$RuCl_2$(cym)]$_2$ with [Au_2Cl_2(dppb)$_2$] in dichloromethane under nitrogen, affording a red crystalline product (Scheme 1). Further details are provided in Section 3.3.

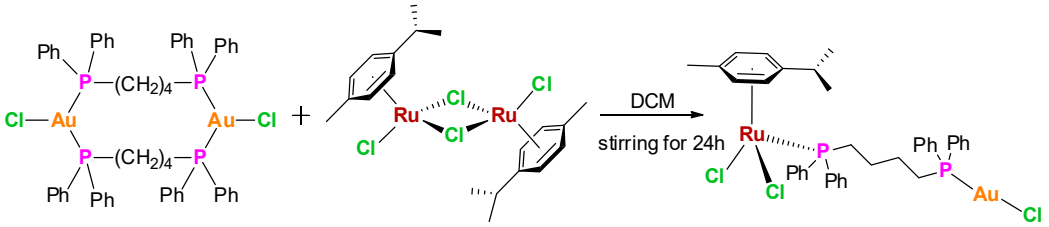

Scheme 1. Synthesis of [(cym)Cl_2Ru-μ-dppb-AuCl] (AuRu).

2.2. Molecular and Crystal Structure

The molecular structure of the AuRu complex is depicted in Figure 1, while the crystallographic parameters and bond lengths and angles are presented in Table 1 and Table 2, respectively. The AuRu complex crystallizes in the *P*-1 space group with two complex molecules per unit cell. The asymmetric unit features one molecule of the complex and two co-crystallized molecules of dichloromethane. Structurally, the complex is heterobimetallic, consisting of coordinated ruthenium(II) and gold(I) centers mutually connected by the 1,4-bis(diphenylphosphino)butane. The coordination environment around the gold(I) center is nearly linear, a geometry routinely observed for Au(I) complexes. One coordination site is occupied by a phosphorus atom from the bridging diphosphine ligand, and the other by the chlorine. The ruthenium(II) ion resides in the center of a pseudo-octahedral coordination sphere, forming a three-legged piano-stool arrangement typical of half-sandwich complexes. In this geometry, three coordination sites are occupied by the η^6-bound cimene ligand, two are taken up by chloride ions, and the remaining site is occupied by the phosphorus atom of the bridging diphosphine.

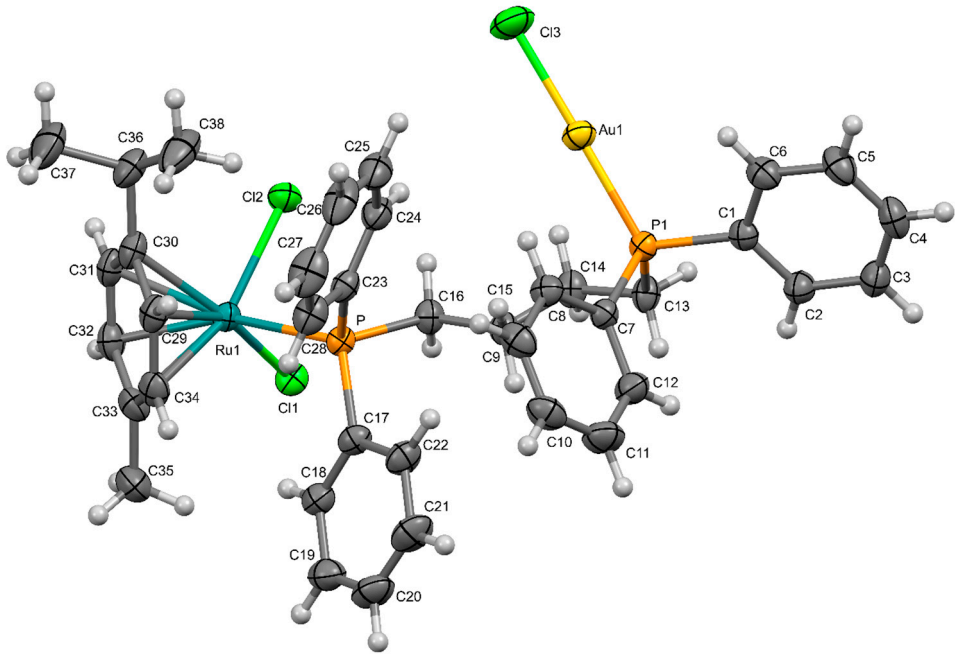

Figure 1. ORTEP representation of the molecular structure of the AuRu complex. Two co-crystallized dichloromethane molecules are omitted for clarity. Thermal ellipsoids are given at the 30% probability level.

Table 1. Crystallographic data for the AuRu complex.

Structure	AuRu
Brutto form.	$C_{40}H_{45}AuCl_7P_2Ru$
Mr ($gmol^{-1}$)	1133.88
Crystal color and habit	translucent light orange prism
Cryst. (mm)	0.15 × 0.09 × 0.07
F (000)	1114
μ (mm^{-1})	1.688
Space group	*P*-1
a (Å)	10.90240(10)
b (Å)	14.7132(2)
c (Å)	15.2437(2)
α (°)	94.9940(10)
β (°)	99.2710(10)
γ (°)	110.6020(10)
V ($Å^3$)	2231.44(5)
Z	2
R_{int}	0.0524
R_σ	0.0474
θ max (°)	79.703
Unique	9465
Obs. [I > 2σ(I)]	8483
Parameters	460
R_1 [I > 2σ(I)]	0.1185
wR_2, all	0.1156
S	0.969
ρ_{max}, ρ_{min}($eÅ^{-3}$)	1.717; −1.367

Table 2. Coordination sphere geometry around Ru and Au in the AuRu complex.

AuRu			
Distances	**Å**	**Angles**	°
C29–Ru1	2.184(6)	C34–Ru1–C29	37.9(3)
C30–Ru1	2.224(6)	C34–Ru1–C33	36.8(3)
C31–Ru1	2.240(6)	C29–Ru1–C33	67.7(3)
C32–Ru1	2.239(6)	C34–Ru1–C30	67.8(3)
C33–Ru1	2.221(6)	C29–Ru1–C30	37.4(2)
C34–Ru1	2.176(6)	C33–Ru1–C30	80.5(3)
P–Ru1	2.3592(14)	C34–Ru1–C32	66.2(3)
Cl1–Ru1	2.4213(14)	C29–Ru1–C32	78.6(3)
Cl2–Ru1	2.4104(16)	C33–Ru1–C32	37.5(3)
Cl3–Au1	2.2798(19)	C30–Ru1–C32	66.7(3)
P1–Au1	2.2311(14)	C34–Ru1–C31	78.1(3)
		C29–Ru1–C31	66.7(2)
		C33–Ru1–C31	66.3(3)
		C30–Ru1–C31	37.8(2)
		C32–Ru1–C31	35.4(3)
		C34 Ru1–P	95.55(18)
		C29–Ru1–P	94.65(17)
		C33–Ru1–P	120.5(2)
		C30–Ru1–P	119.42(16)
		C32–Ru1–P	158.0(2)
		C31–Ru1–P	157.08(18)
		C34–Ru1–Cl2	154.9(2)

Table 2. *Cont.*

AuRu			
Distances	**Å**	**Angles**	°
		C29–Ru1–Cl2	117.08(19)
		C33–Ru1–Cl2	152.4(2)
		C30–Ru1–Cl2	89.20(19)
		C32–Ru1–Cl2	114.9(2)
		C31–Ru1–Cl2	89.98(19)
		P–Ru1–Cl2	86.90(5)
		C34–Ru1–Cl1	116.9(2)
		C29–Ru1–Cl1	154.71(19)
		C33–Ru1–Cl1	90.58(19)
		C30–Ru1–Cl1	155.14(16)
		C32–Ru1–Cl1	92.15(18)
		C31–Ru1–Cl1	117.50(18)
		P–Ru1–Cl1	85.12(5)
		Cl2–Ru1–Cl1	88.18(6)
		P1–Au1–Cl3	179.39(8)

2.3. Chemical and Spectroscopic Characterization

Elemental analysis is in good agreement with the expected formulation and indicates high purity of the bulk AuRu sample. This was further supported by spectroscopic data. Additional characterization was carried out by a combination of 1D and 2D NMR, infrared and electronic spectroscopy, as well as conductivity measurements, all of which confirmed the anticipated structure.

The formation of the AuRu complex in the solution was confirmed by comparing the spectral signal shifts of the free ligand dppb and the Ru(dppb) precursor with those of the final AuRu complex (Figure 2). Upon coordination with Ru(II) ions, the ligand signals become deshielded. When one of the two Ru(II) ions was subsequently replaced by Au(I), the molecular symmetry was disrupted, leading to the expected increase in the number of observable signals. All signals of the dppb ligand, the *p*-cymene moiety, and the phenyl groups were assigned based on the chemical shifts (δ/ppm), multiplicities (s, d, m), and coupling constants (J/Hz) obtained from 1D NMR spectra, as well as the cross-peaks observed in 2D NMR spectra.

The assignment of the dppb chain in the AuRu complex was confirmed by the H-1′-H-7/8 cross-peak observed in the ^{1}H-^{1}H NOESY spectrum (Figure 3A). Similarly, the phenyl groups attached to the phosphorus atoms were assigned by the H1′-C-1″ cross peaks identified in the ^{1}H-^{13}C HMBC spectrum (Figure 3B).

The phosphorus signals in the AuRu complex might be assigned by comparing its chemical shifts in the ^{31}P NMR spectrum with those from the Ru(dppb) complex, in which only ruthenium ions were used for complexation, and with a phosphorus chemical shift of the free dppb ligand (Figure 4). All NMR data are available in the Supplementary Materials.

Further characterization, including infrared and electronic spectra as well as conductivity measurements, is consistent with literature data for similar compounds [38–40] and is provided in the Electronic Supplementary Materials associated with this article.

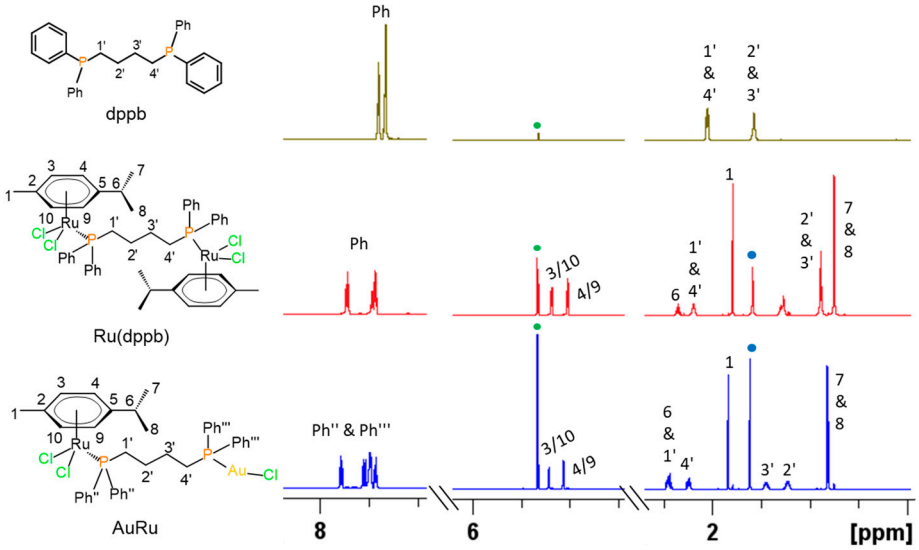

Figure 2. Differences in recorded 600 MHz ^{1}H NMR spectra of dppb, Ru(dppb) and AuRu ligands that confirm the formation of the complex. The green dot indicates the solvent signal (CD_2Cl_2-d_2), while the blue dot corresponds to residual water present in the solvent.

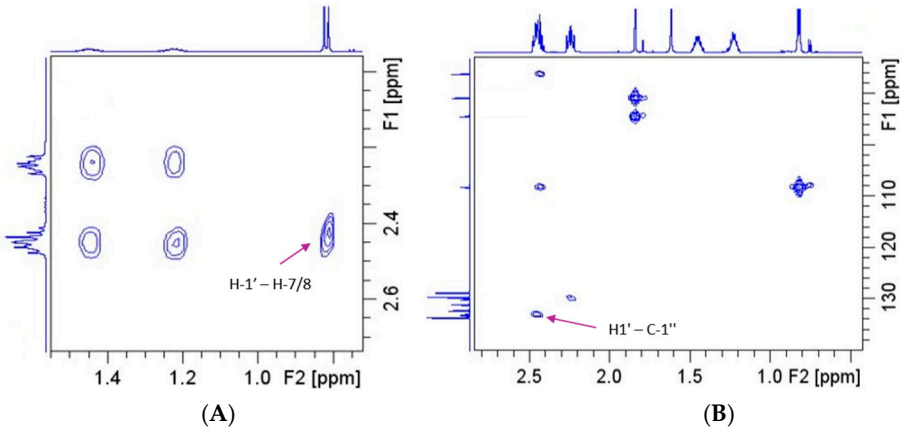

Figure 3. (**A**) ^{1}H-^{1}H NOESY and (**B**) ^{1}H-^{13}C HMBC spectrum of AuRu with key cross-signals for molecule assignment indicated (^{1}H: 600 MHz; ^{13}C: 150 MHz, CD_2Cl_2-d_2).

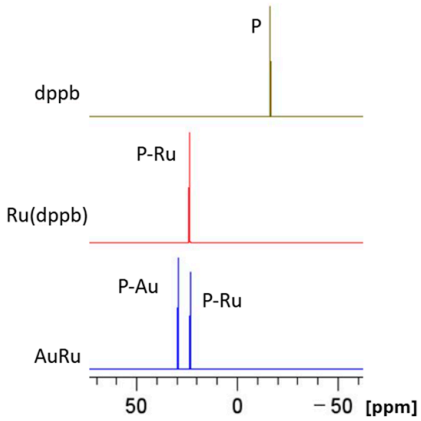

Figure 4. Comparison of the 243 MHz ^{31}P spectra of the free ligand dppb and in the complex with ruthenium (Ru(dppb)) and ruthenium-gold (AuRu) in CD_2Cl_2-d_2.

Behavior in Aqueous Solution

Understanding the solution behavior of bioactive metal complexes under aqueous conditions is crucial for rationalizing their potential reactivity and activation pathways in physiological environments. The stability of the AuRu complex was assessed in aqueous solution after initial dissolution in DMSO by monitoring its transformation using UV–Vis spectroscopy. Spectra were acquired at five-minute intervals during the first hour, with a further measurement at 24 h (Figure 5). Pseudo-first-order kinetic treatment (upper inset) yielded a rate constant k = 7.36 × 10^{-2} min^{-1} ($k \approx 1.23 \times 10^{-3}$ s^{-1}), giving a half-life $t_{1/2} \approx 9.4$ min. This kinetic profile is consistent with values reported for classic Ru–arene dichlorido complexes. For example, RAPTA-C ([Ru(η^6-*p*-cymene)Cl_2(PTA)]) exhibits rapid aquation under low chloride conditions, with a reported half-life of only a few minutes (approx. $t_{1/2} \lesssim 5$ min) under physiological ionic strength [41]. Other Ru-arene systems, studied in UV–Vis kinetic experiments, show aquation rate constants in the range ~1.2 × 10^{-3} to 2.6 × 10^{-3} s^{-1} (i.e., $t_{1/2} \approx$ 4–10 min) [42].

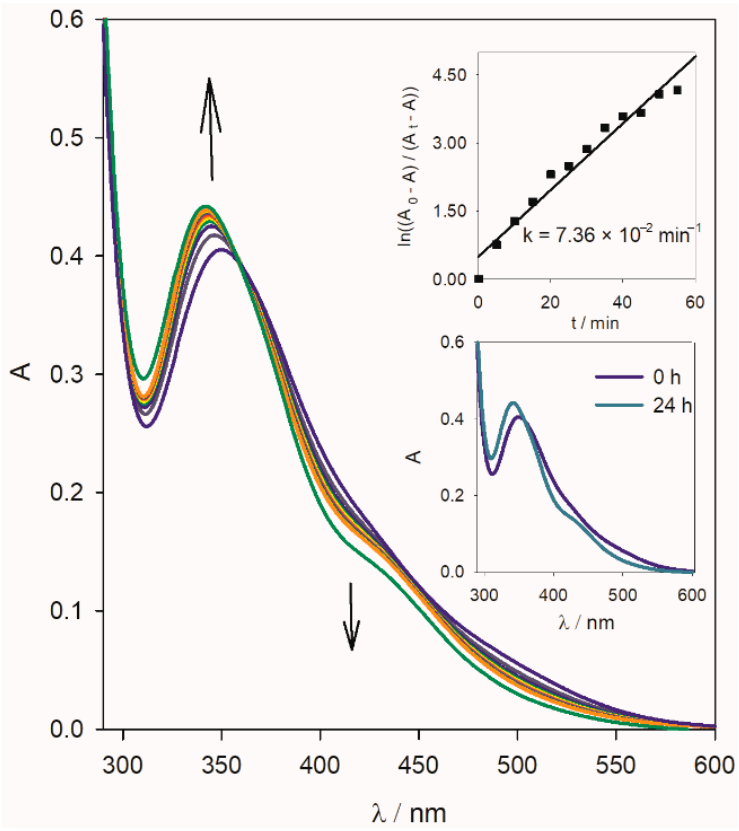

Figure 5. Electronic absorption spectra of the AuRu complex (50 µM, H_2O/DMSO 90:10 *v*/*v*, 25 °C, quartz cuvette 1 cm) were recorded at five-minute intervals during the first hour and after 24 h. Top inset: pseudo-first-order kinetic plot λ_{max} = 350 nm. Bottom inset: comparison of the initial spectrum with that recorded after 24 h, illustrating the extent of the spectral changes.

The aquation of the AuRu complex manifests as a decrease in the intensity of the LMCT band attributed to chloride-to-Ru(II) charge transfer and a clean isosbestic point around ~360 nm, suggesting a well-defined two-species conversion. This behavior and the kinetic similarity confirm that the Ru center in AuRu behaves analogously to classical Ru–arene dichlorido complexes, undergoing chloride substitution in water [41,42]. The slightly slower observed rate compared to RAPTA-C likely reflects the stabilizing influence of the µ-dppb–Au(I) bridge and lower solvation, which may hinder chloride lability without altering the fundamental mechanistic pathway. Scheme 2 illustrates the proposed aquatation pathway of the AuRu complex.

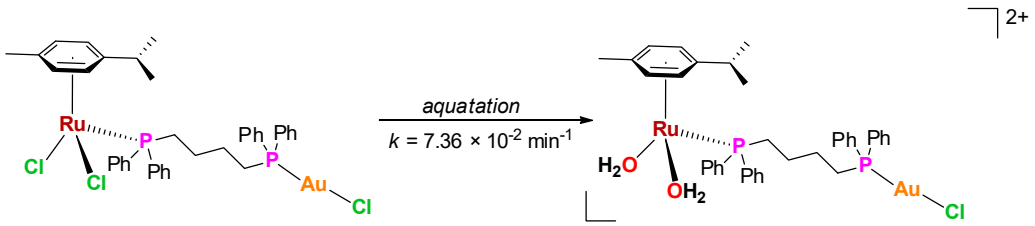

Scheme 2. Proposed aquatation pathway of the AuRu complex.

While electronic spectroscopy indicates substitution of the chlorido ligands at the ruthenium center, it does not provide reliable information on whether the dppb bridge remains intact or if the AuRu complex retains the structural integrity of the Ru–μ-dppb–Au framework. To gain further insight into these potential changes, we applied ^{31}P NMR spectroscopy in dry DMSO-d6 and in the DMSO-d6/D_2O mixture (Figure 6). The addition of water to the solution of the AuRu complex in DMSO-d6 results in a slight change in the chemical shift signal of the phosphorus atom bound to both metal ions. At %D_2O/DMSO = 9%, two sets of signals are visible in the spectrum, which change the ratio upon further titration, and finally, at %D_2O/DMSO = 50%, only one set is present. The signal of the phosphorus bound to the gold ion is shielded by −0.84 ppm, while the change in the signal of the phosphorus bound to ruthenium is greater and deshielded by 1.88 ppm. The above-mentioned changes in the chemical shift of the signal indicate that the addition of water leads to hydrolysis, to which chloride ions are susceptible. Furthermore, these chemical shifts of the phosphorus remain unchanged upon addition of DMSO-d6, supporting the hypothesis that an irreversible replacement of the chloride ion by water has occurred in the AuRu complex. No signals corresponding to the chemical shift of the pure dppb ligand in the ^{31}P NMR spectrum were observed upon water addition. These results indicate that no significant structural rearrangements occur in solutions and that the μ-dppb bridge is preserved.

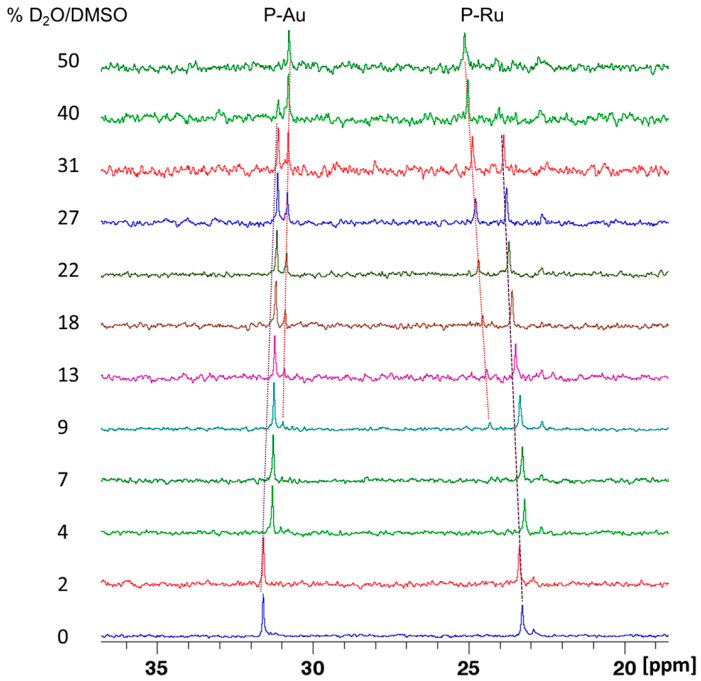

Figure 6. Changes in the ^{31}P NMR spectra of the AuRu during titration of the DMSO-d6 complex solution with D_2O in the ratios indicated in the figure.

2.4. Interaction with BSA

In biological media, albumin binding is a major determinant of metallodrug distribution, and investigating how metal complexes bind to BSA provides insights into their bioavailability, stability, and potential toxicity [43]. The interactions between BSA and the synthesized AuRu complex, as well as the individual Au(dppb) and Ru(dppb) complexes, were investigated using spectrofluorimetric titration [44]. A hypsochromic shift and fluorescence quenching of BSA were observed upon addition of these complexes, and the quenching effect was quantitatively analyzed using the Stern–Volmer equation.

Figure 7 displays the emission spectrum of BSA at a fixed concentration upon the gradual addition of AuRu, while the corresponding spectra for Au(dppb) and Ru(dppb) are provided in the Supplementary Materials. Table 3 presents data on graphically determined fluorescence quenching constants, binding constants, and the number of binding sites for all three investigated complexes. The bimolecular fluorescence quenching constants (k_q) were in the range of 10^{12}–10^{13} M^{-1} s^{-1}, and are higher than the diffusion-controlled quenching limit (2×10^{10} M^{-1} s^{-1}), indicating the formation of non-fluorescent complexes between BSA and all investigated compounds [45].

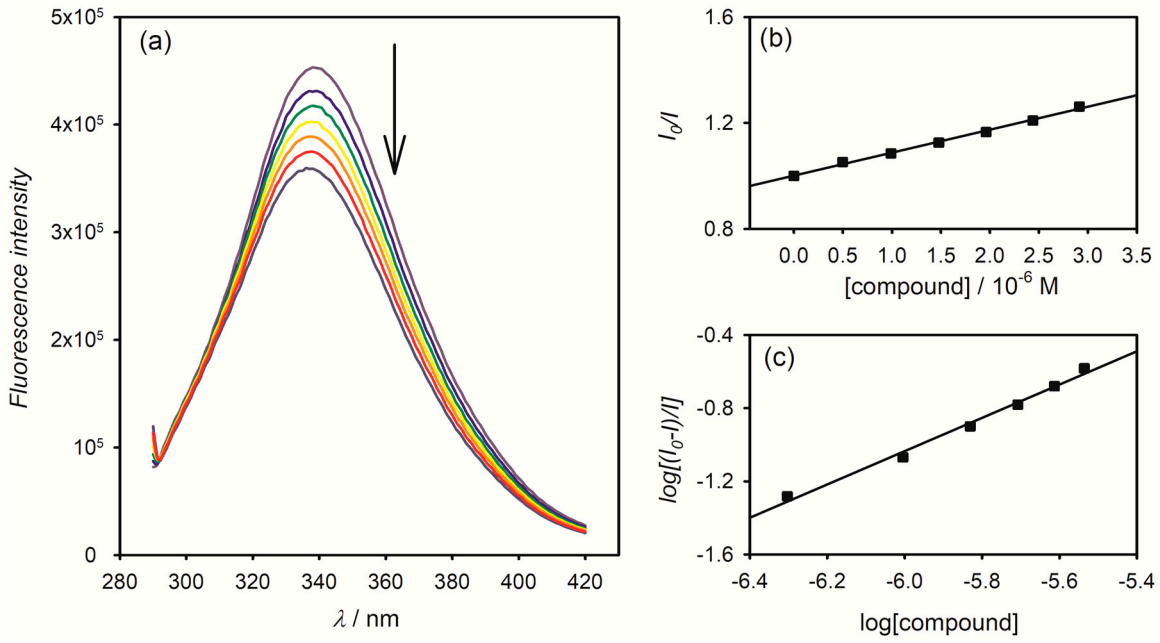

Figure 7. Interaction of AuRu with BSA in 50 mM phosphate buffer pH 7.42: (**a**) fluorescence quenching of BSA (2.93×10^{-5} M) in the presence of increasing concentration of AuRu; (**b**) graphical determination of Stern–Volmer constant; (**c**) graphical determination of binding constant and the number of binding sites.

Table 3. Data on the interaction of complexes Au(dppb), Ru(dppb), and AuRu with BSA.

Compound	$K_{SV}/10^5$ M^{-1}	$k_q/10^{13}$ M^{-1} s^{-1}	$K_b/10^4$ M^{-1}	*n*
Au(dppb)	1.49	1.49	14.1	1.00
Ru(dppb)	1.07	1.07	0.05	0.58
AuRu	0.87	0.87	2.66	0.91

Among the tested species, the Au(dppb) complex exhibited the highest apparent binding constant toward BSA ($K_b = 1.41 \times 10^5$ M^{-1}), suggesting strong affinity. However, such a value must be interpreted with caution, since it is well established that many gold(I) complexes containing chlorido ligands or thioglucose bind irreversibly and selectively

to the Cys34 residue of albumin through Au–S bond formation [46,47]. In such cases, binding constants derived from fluorescence quenching do not represent a true reversible equilibrium, but rather the kinetics of covalent metalation. In contrast, Ru(dppb) displayed a markedly lower value (K_b = 5.12 × 10^2 M^{-1}), consistent with very weak binding. This constant is significantly smaller than those reported for RAPTA-C and related Ru–arene chlorido complexes, which typically bind to BSA/HSA with conditional constants in the range of 10^4–10^5 M^{-1} [48–50].

The AuRu complex showed an intermediate binding constant of 2.66 × 10^4 M^{-1}, indicative of moderate affinity toward BSA. Its binding is clearly weaker than that of Au(dppb), yet markedly stronger than Ru(dppb), and this behavior is consistent with dual contributions from the Au and Ru moieties. However, as noted above, this value should be interpreted with caution, since the Au(I) fragment in AuRu can undergo irreversible metalation at albumin cysteine residues, meaning that the measured constant may partly reflect covalent adduct formation rather than purely reversible binding. It should also be emphasized that direct comparison of binding constants across systems is inherently difficult since albumin interactions are highly sensitive to ionic strength, buffer composition, pH, temperature, and even the chosen spectroscopic method [50]. Although the relative trend (Au > AuRu > Ru) is meaningful, the absolute values should be considered only as apparent affinities rather than precise thermodynamic constants.

The number of binding sites for both Au(dppb) and AuRu complexes was close to 1, implying that a single molecule of the complex interacts with one primary binding site on the protein. In the case of Ru(dppb), the binding site number was approximately 0.5.

The Förster resonance energy transfer (FRET) theory was employed to evaluate the non-radiative energy transfer between BSA, acting as the fluorophore, and the investigated complexes [51]. The spectral overlap between the emission of BSA and the absorption of the AuRu complex is shown in Figure 8 (with analogous data for the other complexes provided in the Supplementary Materials), which enabled the calculation of the overlap integral (J) [52].

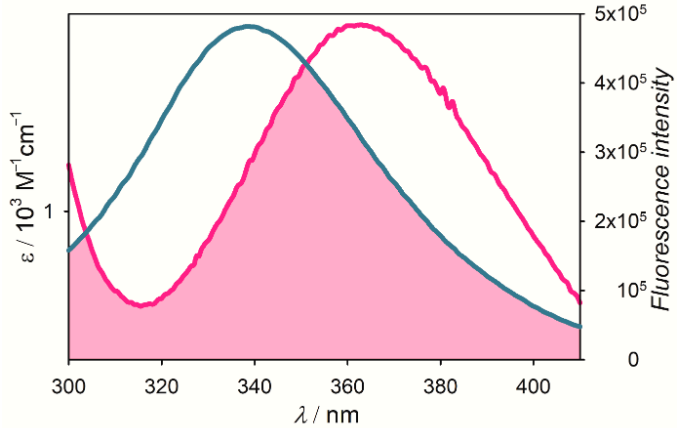

Figure 8. Overlap of the BSA emission spectrum (blue) and absorption spectrum of AuRu (pink).

Based on this, the Förster distance (R_0) was determined according to established methods. The energy transfer efficiency (E) was derived from the fluorescence intensities of BSA measured in the presence and absence of the complexes, and subsequently used to estimate the actual donor–acceptor distance (r) at which the energy transfer occurs [53].

Since the calculated distances fulfill the condition $0.5R_0 < r < 1.5R_0$, the values listed in Table 4 support a static quenching mechanism and indicate that fluorescence attenuation arises from non-radiative energy transfer between BSA and the studied complexes [38].

Table 4. FRET analysis data on BSA—complexes Au(dppb), Ru(dppb), and AuRu.

Compound	J/cm^3/M	E	R_0/nm	r/nm
Au(dppb)	3.17×10^{-16}	0.30	1.38	1.59
Ru(dppb)	2.82×10^{-15}	0.25	1.99	2.38
AuRu	1.62×10^{-15}	0.21	1.81	2.26

2.5. In Vivo Testing

In vivo testing of the AuRu complex in Wistar rats was undertaken to establish its toxicological profile, a key aspect often overlooked in studies focusing solely on anticancer or antimicrobial properties of metal complexes. Confirming the systemic safety prior to mechanistic or therapeutic evaluation provides a solid foundation for future investigations, especially given the structural features of the complex that suggest promising biological activity.

Figure 9 presents an overview and the endpoints of the experiment conducted on Wistar rats, in which the effects of the AuRu complex on biochemical, hematological, and histological parameters were examined.

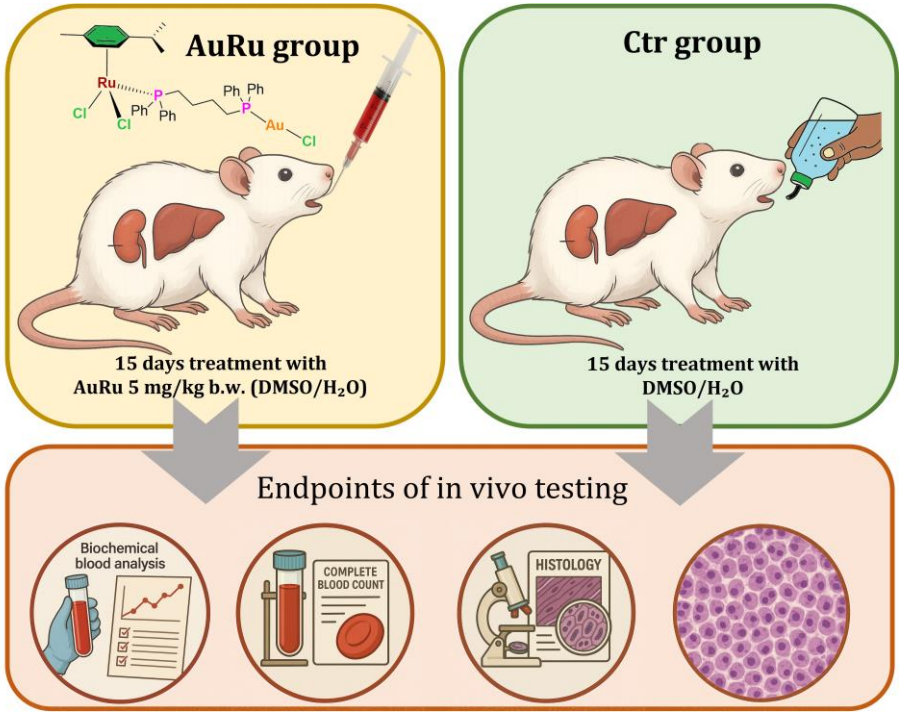

Figure 9. Overview and endpoints of in vivo testing.

The mean value of total serum proteins was statistically significantly lower in the control group, which indicates a certain effect of the AuRu complex on liver function in terms of protein synthesis and metabolism. Due to impairments of the liver tissue, protein synthesis is reduced. The observed difference may still suggest that the investigated complex affects the metabolism in the liver, not only of the proteins, but also of carbohydrates and lipids, taking into account the fact that the glucose level was also found to increase in the AuRu group (Figure 10B). However, the results of the liver functional tests, namely AST and ALT, along with a finding of almost completely preserved liver histoarchitecture in the AuRu group of rats (Figure 10A) implies that the substance, when applied in a chosen dose, was not hepatotoxic.

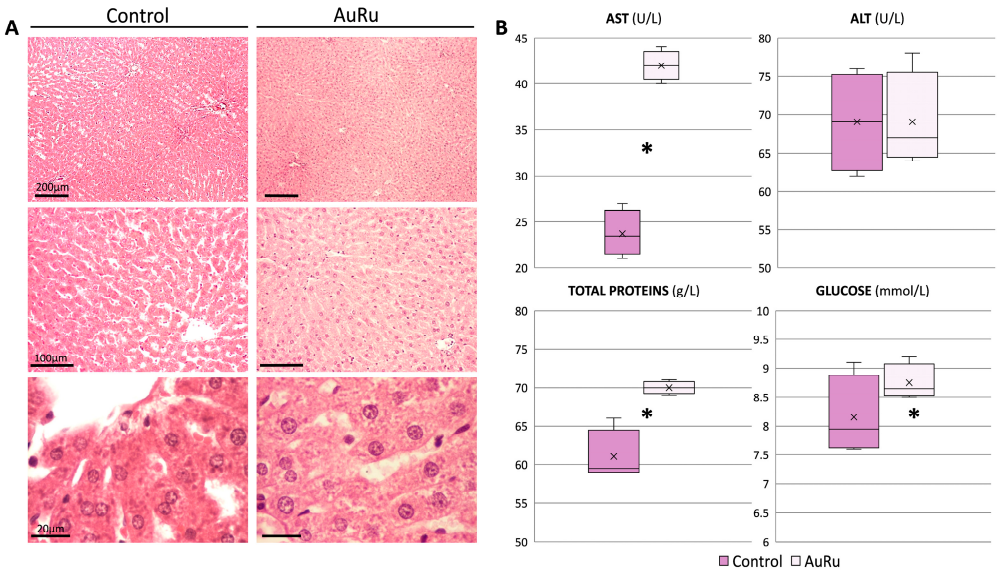

Figure 10. Evaluation of hepatotoxicity after AuRu application in rats. (**A**) Representative photomicrographs of the liver—clearly visible lobular architecture, sinusoids, and radiating hepatocyte cords in the control group of rats and preserved histoarchitecture in the AuRu group with mild granular or slight hydropic degeneration of the hepatocyte cytoplasm (HE); (**B**) Comparison between AST and ALT activities, total proteins and glucose concentrations in the sera of the control (purple) and AuRu group (white). * $p < 0.05$.

Histological analysis of the kidneys from the control group showed normal, completely preserved structural elements, while in the AuRu group, some alterations were noted in the sense of sporadic renal corpuscle lobulation and obliteration of the intracapsular space. Also, occasionally, proximal tubules contained eosinophilic casts; their cells seemed swollen and partially degenerated, while distal tubules appeared relatively normal (Figure 11A). The renal functional tests for both groups of animals were in a reference range (Figure 11B) and exhibited no statistically significant differences, thus indicating that the observed histological changes were mild and potentially reversible. In summary, the AuRu complex investigated in our study did not exhibit significant nephrotoxicity. Similar results to ours were obtained in the research of Ahmed et al. [54]. Serum glucose levels were significantly higher in the AuRu group compared to the control group, suggesting that the complex may affect pancreatic endocrine function and insulin secretion. Some ruthenium complexes, such as the ruthenium Schiff base complex, have been shown to possess antidiabetic properties through anti-inflammatory, antioxidant, and vasodilation mechanisms [55]. Lower glucose levels in these cases likely reflect improved insulin sensitivity induced by the metal complex, suggesting therapeutic potential for pre-diabetic patients through enhanced glucose utilization and homeostasis. [55]. AST and ALT levels in the AuRu group remained within normal limits, suggesting minimal hepatotoxicity, as liver injury would otherwise elevate these enzymes. According to Hou et al., the ruthenium metal complex TQ-5 and its ligand prevented iNOS, TNF-α, IL-1β, and LPS-induced liver damage in mice by preventing the production of these molecules and phosphorylating NF-κBp65 [56]. These in vivo results are consistent with our research in terms of the possible hepatoprotective effects of AuRu complexes.

LDH is an enzyme found in the liver, heart, kidneys, skeletal muscles, and erythrocytes, and catalyzes the interconversion of lactate and pyruvate; therefore, it is not strictly organospecific. However, elevated values can correlate with certain parameters in the body that show potential damage to a certain tissue or organ. The current study revealed that LDH was higher in the Ctr group (Table 5).

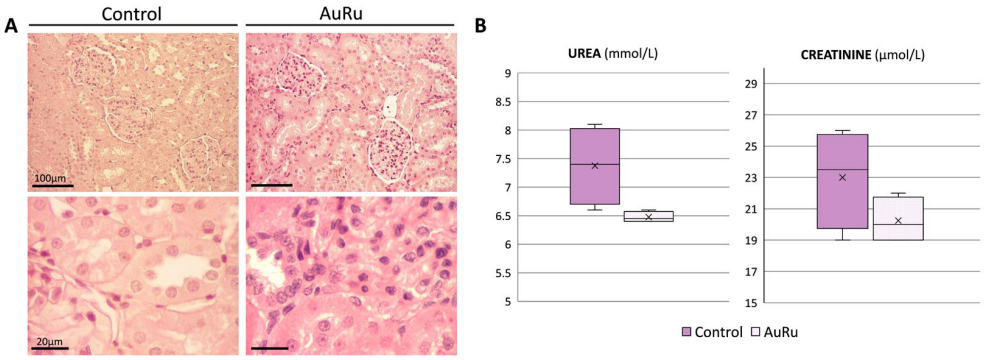

Figure 11. Evaluation of nephrotoxicity after AuRu application in rats. (**A**) Histological analysis of the kidneys of the control group revealed normal histoarchitecture, while in the AuRu group, the intracapsular space of the renal corpuscles was occasionally found obliterated; proximal tubules contained casts, and their cells seemed swollen and partially degenerated (HE). (**B**) Comparative evaluation of serum urea and creatinine concentration between the control (purple) and AuRu group of rats (white).

Table 5. Results of minerals and enzymes.

	AuRu	Ctr	Sig.
SODIUM (mmol/L)	149.75 ± 2.63	155.66 ± 9.99	0.03
CHLORIDE (mmol/L)	101.25 ± 0.96	100.16 ± 5.84	0.12
LDH (U/L)	451.5 ± 112.80	599.83 ± 182.3	0.01
CK (U/L)	342.25 ± 29.01	297.83 ± 116.97	0.03

Creatine kinase (CK) is an enzyme that catalyzes the conversion of creatine and adenosine triphosphate (ATP) to phosphocreatine and adenosine diphosphate (ADP). Depending on the type and level of CK, skeletal muscle, heart, or brain damage or disease is possible. Manibusan et al. found that many types of harmful substances induce free radical production and cause cardiac myocyte rupture and membrane peroxidation, which raises serum CK levels [57]. Among currently found adverse effects, the research of Ciftci et al. revealed that ruthenium(II) and gold(I)-NHC complex-treated rats that received both Ru(II) and Au(I) complexes significantly had oxidative, histological, spermatological, and hormonal impairments [58]. These substances have the potential to be hazardous to the male reproductive system and result in infertility when used for cancer treatments.

The AuRu group showed a small reduction in serum sodium compared with controls, while chloride levels remained unchanged (Table 5). Although the *p*-value suggests statistical significance, the effect appears minor when taking into account the standard deviations, and is unlikely to represent a substantial physiological change.

WBC count was higher in the Ctr group in comparison to the AuRu-treated rats (Table 6). AuRu treatment had a strong effect on the decrease in the number of leukocytes, which implies the potential influence of this complex on leukopoiesis in the bone marrow. The number of LYM and GRAN was significantly lower in the AuRu group than in the control group. Ruthenium and gold complexes are clinically used for immune suppression, as they have antimigratory and antiangiogenic properties, and gold complexes showed effects on the immune cells and immune checkpoints [31]. They induce the release of pro-inflammatory mediators such as IL-8 from DC, PBMC, and THP-1 cells [59]. Slightly reduced values of RBC and HB suggest the potential development of possible anemia during subchronic or chronic AuRu treatment; platelet numbers were slightly decreased in the AuRu group, suggesting that it has thrombocytopenic effects. However, these results were within reference range. Since ruthenium complexes show promise as substitutes for conventional anticancer drugs [60], they show apoptotic mechanisms towards proliferating

cancer cells (and consequently leukocytes and platelets, which leads to their decline). Certain gold complexes, such as derivatives of gold(I) or gold(III), have shown promise as cytotoxic agents, frequently overcoming cisplatin resistance in particular cancer types [61,62]. Hematological indices (MCV, MCH, and MCHC) were uniform in both groups.

Table 6. Results of hematological analysis.

	AuRu	Ctr	Sig.
WBC ($\times 10^3/\mu L$)	3.23 ± 0.22	7.11 ± 0.58	0.00
LYMPH ($\times 10^3/\mu L$)	1.41 ± 0.55	5.23 ± 0.51	0.00
GRAN ($\times 10^3/\mu L$)	0.41 ± 0.15	1.83 ± 0.83	0.00
RBC ($\times 10^6/\mu L$)	6.73 ± 1.43	7.14 ± 0.45	0.30
HGB (g/dL)	14.4 ± 1.09	14.42 ± 0.51	0.93
HCT (%)	39.00 ± 4.96	37.92 ± 1.17	0.00
MCV (fL)	57.43 ± 9.03	52.58 ± 4.25	0.25
MCH (pg)	22.33 ± 7.31	19.21 ± 0.58	0.28
MCHC (g/dL)	38.05 ± 5.68	37.24 ± 2.29	0.11
PLT ($\times 10^3/\mu L$)	404.8 ± 110.84	412.16 ± 22.28	0.13

The effects of the AuRu complex on the nuclei of hepatocytes are presented in Figure 12. In the group treated with the AuRu complex, the shape and structure of hepatocytes' nuclei are preserved, although there are minor structural changes in the karyoplasm; the granular karyoplasm is looser, with the presence of 3–4 nucleoli. Zhang et al. have reported a ruthenium-gold-peptide conjugate for the selective therapy of hepatocellular carcinoma and similar changes in nuclei [63]. Current research showed that the AuRu complex had some protective and beneficial properties on the shape and size of nuclei of hepatocytes; it reduced the percentage of altered nuclei in terms of cytogenetic aberrations. The karyoplasm is granular; from the periphery to the center, genetic changes are more pronounced in the AuRu group. The control group did not show any aberrant morphological features in terms of the shape or size of nuclei.

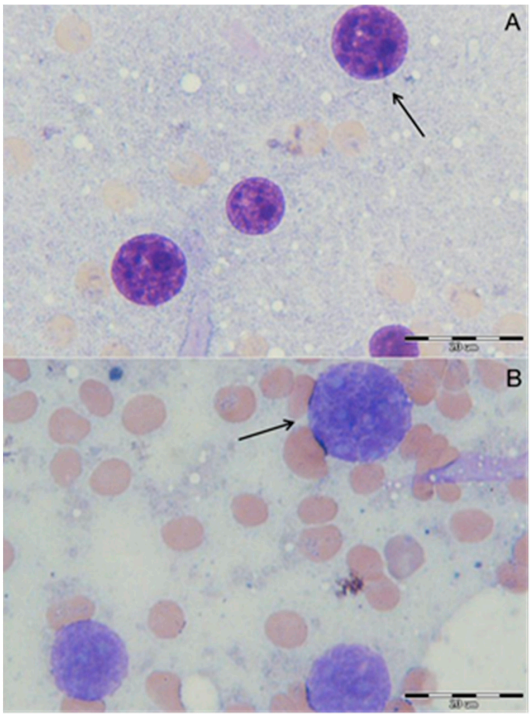

Figure 12. Hepatocyte nuclei morphology observation. (**A**) AuRu complex, (**B**) Control group; black arrows show nuclei of hepatocytes with normal morphology.

The AuRu complex appears to exert only minor effects on hepatocyte nuclei and on biochemical and hematological parameters, suggesting its potential as a biologically active substance with limited harmful impact. However, careful dosing and further investigation of possible contraindications are necessary to clarify their overall effects on the organism's physiological state.

3. Experimental Section

3.1. Chemicals

Unless otherwise indicated, all substances used for synthesis and interaction monitoring were of analytical grade. Tetrachloroauric acid trihydrate, ruthenium trichloride hydrate, tetrahydrothiophene, 1,4-bis(diphenylphosphino)butane (dppb), and α-phellandrene were purchased from Sigma-Aldrich and used as received. Ruthenium complexes $[RuCl_2(p\text{-cymene})]_2$ [64] and $[\{RuCl_2(p\text{-cymene})\}_2(\mu\text{-dppb})]$ [65] were prepared according to published procedures. Likewise, the gold precursors [Au(tht)Cl] [66] and $[Au_2Cl_2(dppb)_2]$ [2,67] were obtained following reported synthetic protocols. All precursor complexes have elemental analysis or spectroscopic data consistent with those previously reported. All solvents were used as received from the supplier, while dimethylsulfoxide was dried over molecular sieves (3 Å). Lyophilized powder of Bovine serum albumin (BSA, $\geq$98%) was acquired from Sigma-Aldrich.

3.2. Physical Measurements

The elemental composition was determined using a Perkin Elmer 2400 Series II CHNS analyzer. The ruthenium content was determined spectrophotometrically [68]. Infrared spectra were recorded using the ATR technique on a Perkin Elmer UATR Two in transmission mode. Electronic spectra were measured using a Perkin Elmer Bio Lambda 35. A Perkin Elmer LS 55 Luminescence spectrophotometer was used for conducting fluorescence measurements. NMR spectra were recorded with a Bruker AV600 spectrometer (Bruker BioSpin GmbH, Rheinstetten, Germany) equipped with a 14 T superconducting magnet and a 5 mm diameter double resonance ATM broadband probe PABBO. The standard ^{1}H and proton-decoupled $^{13}C\{^{1}H\}$ NMR spectra were recorded at 600.130 and 150.903 MHz, respectively. The ^{31}P NMR spectra were recorded at 242.925 MHz. The chemical shifts (δ/ppm) of the ^{1}H and ^{13}C spectra were referenced to the solvent signal: CD_2Cl_2-d_2 (^{1}H: δ = 5.32 ppm; ^{13}C: δ = 54.00 ppm), and the chemical shift scale of the ^{31}P spectrum was referenced to the external standard signal of 85% H_3PO_4 (^{31}P: δ = 0.0 ppm). The assignment of the ^{1}H and ^{13}C signals in the recorded NMR spectra was confirmed by cross peaks in the 2D spectra: ^{1}H-^{1}H COSY (Correlation Spectroscopy), ^{1}H-^{1}H NOESY (Nuclear Overhauser Effect Spectroscopy), ^{1}H-^{13}C HMQC (Heteronuclear Multiple Quantum Coherence), and ^{1}H-^{13}C HMBC (Heteronuclear Multiple Bond Correlation).

3.3. Synthesis of [(cym)Cl_2Ru-μ-dppb-AuCl] (AuRu)

A solution of $[RuCl_2(cym)]_2$ (172 mg, 0.28 mmol) in 25 mL of dichloromethane (DCM) was prepared under a nitrogen atmosphere. To this solution, $[Au_2Cl_2(dppb)_2]$ (370 mg, 0.28 mmol) was added in one portion, and the reaction mixture was stirred at room temperature for 24 h. During this time, a clear red solution was obtained. Upon the completion of the reaction, the solvent was removed under reduced pressure using a rotary evaporator. The resulting red residue was redissolved in a small volume of DCM (5 mL) and filtered through filter paper to remove any insoluble impurities. The bulk sample of AuRu was obtained by slowly adding n-hexane to a vigorously stirred dichloromethane solution of the product, affording a red microcrystalline solid. The solid was collected by filtration, washed with cold diethyl ether and methanol, and dried under vacuum. Red crystals

suitable for single-crystal X-ray diffraction (SCXRD) were obtained by layering n-hexane to the DCM solution of the complex at room temperature over 72 h.

trichlorido-1κ*Cl*,2κ^2*Cl*-{μ-1,4-bis(diphenylphosphino)butane-1κ*P*:2κ*P*′}(η^6-*p*-cymene-1η^6)ruthenium(II)gold(I). [(cym)Cl_2Ru-μ-dppb-AuCl] (AuRu). Orange-red powder and crystals. Yield: 347 mg (66%). *Anal. Calc.* (%) for $C_{38}H_{42}AuCl_3P_2Ru$ (Mr = 965.09): C, 47.29; H, 4.39; Ru, 10.47. *Found* (%): C, 47.56; H, 4.57; Ru, 10.23. ^{1}H NMR (600.130 MHz, 25 °C, CD_2Cl_2-d_2): *δ* 7.81–7.76 (4H, m, H-2″), 7.57–7.52 (4H, m, H-2‴), 7.51–7.46 (8H, m, H-3″/4″/4‴), 7.45–7.41 (4H, m, H-3‴), 5.21 (2H, d, *J* = 6.36 Hz, H-3/10), 5.07 (2H, d, *J* = 6.00 Hz, H-4/9), 2.48–2.40 (3H, m, H-6 and H-1′), 2.27–2.21 (2H, m, H-4′), 1.84 (3H, s, CH_3-1), 1.50–1.40 (2H, m, H-3′), 1.27–1.18 (2H, m, H-2′), 0.82 (6H, d, *J* = 6.89 Hz, CH_3-7/8) ppm. ^{13}C NMR (150.903 MHz, 25 °C, CD_2Cl_2-d_2): *δ* 133.8 (4C, d, $J_{C,P}$ = 9 Hz, C-2″), 133.7 (4C, d, $J_{C,P}$ = 13 Hz, C-2‴), 133.2 (2C, d, $J_{C,P}$ = 43 Hz, C-1″), 132.3 (2C, d, $J_{C,P}$ = 3 Hz, C-4‴), 131.2 (2C, d, $J_{C,P}$ = 2 Hz, C-4″), 129.9 (2C, d, $J_{C,P}$ = 60 Hz, C-1‴), 129.7 (4C, d, $J_{C,P}$ = 11 Hz, C-3‴), 128.9 (4C, d, $J_{C,P}$ = 10 Hz, C-3″), 108.3 (1C, C-5), 94.6 (1C, C-2), 90.89 and 90.87 (1C, C-3 and 1C, C-10), 86.25 and 86.22 (1C, C-4 and 1C, C-9), 30.6 (1C, C-6), 28.1 (1C, d, $J_{C,P}$ = 38 Hz, C-4′), 27.2 (1C, dd, $J_{C,P}$ = 12; 3 Hz, C-3′), 24.9 (1C, dd, $J_{C,P}$ = 16; 7 Hz, C-2′), 23.5 (1C, d, $J_{C,P}$ = 29 Hz, C-1′), 21.6 (2C, C-7/8), 17.7 (1C, C-1) ppm. ^{31}P NMR (242.925 MHz, 25 °C, CD_2Cl_2-d_2): *δ* 29.4 (P-Au), 23.2 (P-Ru) ppm. ATR-FTIR ν(cm^{-1}): 3047, 3038 $\nu(C–H)_{aryl}$; 2954, 2931, 2913,2868 $\nu(C–H)_{alkyl}$; 1432 CH_2 scissoring; 1100 $\nu(P–C)_{aryl}$; 848 CH_2 rocking; 797 $\gamma(C–H)_{out\text{-}of\ plane}$ of *p*-cymene aromatic ring; 745, 726, 693 $\gamma(C–H)_{out\text{-}of\text{-}plane}$ of dppb aromatic rings and $\nu(P–C)_{alkyl}$, fingerprint region. UV/Vis (DCM) λmax/nm (log ε): 268 (3.86); 362 (3.16). Λ_M (1 mM, DMSO, 25 °C) = 9.2 S cm^2 mol^{-1}.

3.4. X-Ray Crystallography

The data were collected at ambient temperature using an XtaLAB Synergy diffractometer equipped with a micro-focus sealed X-ray tube (λ = 1.54183 Å). Data processing and unit cell refinement were conducted with CrysAlisPro (Version 1.171.42.62a, Rigaku, 2020), applying a standard multi-scan absorption correction. Structural determination was performed using direct methods in SHELXT [69], followed by full-matrix least-squares refinement on F^2 with SHELXL [70]. Molecular visualizations were generated using MERCURY [71], while molecular geometry calculations and crystal packing analysis were carried out with PLATON [72]. All software used for structure solution, refinement, and visualization is part of the WinGX package [73]. Hydrogen atoms were positioned based on geometric calculations and refined using the riding model.

3.5. Interaction with BSA

The interaction of complexes with BSA was investigated by fluorometric titration at 298 K. For this purpose, a 2.93 × 10^{-5} M working solution of BSA was made in 50 mM phosphate buffer, pH 7.42, while the tested complexes were prepared in DMSO at 1 × 10^{-4} M concentration. The BSA solution (2000 μL, 2.93 × 10^{-5} M) was titrated with successive additions of 10 μL of the complex (0–60 μL), and after each addition, the emission spectrum was recorded at 280–420 nm, with excitation at 278 nm.

3.6. In Vivo Testing—Experimental Protocol

The current research used eight Wistar male rats weighing 198 ± 7.45 g. The Universal Declaration of Animal Welfare, the UNESCO Declaration on the Rights of Animals, and the European Parliament's Directive 2010/63/EU on the protection of animals used for scientific purposes all established the Principles of Laboratory Animal Care, which are adhered to in all animal care procedures.

Two groups of animals were obtained as follows: AuRu complex group (n = 4): animals received AuRu complex daily (dissolved in DMSO, 5 mg/kg b.w.) via oral gavage for a

total period of 15 days. Ctr group (n = 4): rats that were used as a control group; treated with drinking water and DMSO via oral gavage for 15 days. Dosing criteria and exposure time were determined according to the literature [74–77].

3.7. Biochemistry and Hematology

An intraperitoneal dose of xylazine (20 mg/kg) and ketamine (100 mg/kg) was collected for both biochemical and hematological analysis. For the biochemical analysis, 3 mL of blood was centrifuged at 3000 rpm for 10 min at 4 °C to obtain the serum, and, using the Vitros 350 analyzer, the following parameters were measured: total proteins, urea, creatinine, glucose, sodium, chloride, aspartate aminotransferase, alanine aminotransferase, lactate dehydrogenase, and creatine kinase. Hematological parameters that were observed were: white blood cells count (WBC), number of lymphocytes (LYM), number of granulocytes (GRAN), platelets count (PLT), red blood cells count (RBC), hemoglobin concentration (HB), hematocrit value (HCT), and hematological indices: mean corpuscular volume (MCV), mean corpuscular hemoglobin (MCH), and mean corpuscular hemoglobin concentration (MCHC). All biochemical parameters were determined on the Vitros 350 analyzer; hematological parameters were determined on the Mythic 5VET PRO hematological analyzer.

3.8. Hepatocytes Nuclei Morphology Observation

Hepatocytes' nuclei morphology was obtained by the preparation of microscopic slides. Cross-sections of the liver right lobe were done and immersed in sterile saline for 5 min. The touch imprinting method was used to prepare the slides. They were fixed for five minutes in methanol, followed by staining with Giemsa (1:10 diluted with distilled water) for 30 min [78]. Morphological changes of hepatocytes were observed by Olympus DP software using an Olympus microscope BX41 equipped with a DP12 camera.

3.9. Histology

During an autopsy, the liver and kidneys were carefully dissected and macroscopically analyzed. Tissue samples were cut rapidly and fixed in neutral buffered formalin. Formaldehyde-fixed samples further underwent a routine procedure of dehydration, clearing, infiltration, and embedding using an automatic tissue processor (TP1020, Leica, Germany) and an embedding center (MPS/P, SLEE Mainz, Germany). Paraffin-embedded tissue blocks were sectioned into 5 µm thick sections (Microm HM 340E, Thermo Scientific, USA), deparaffinized, rehydrated, and stained with hematoxylin and eosin (HE) according to the manufacturer's protocol (BioGnost Ltd., Croatia). Slides were evaluated under the light microscope (Nikon Eclipse E400, Japan) at 40×, 100×, and 400× magnification in a blinded fashion. The representative photomicrographs were made using a camera connected to the microscope (Nikon DN100, Japan).

3.10. Statistical Analysis

The data was analyzed using SPSS 20.0. One-way ANOVA was utilized to examine significant differences between groups.

4. Conclusions

The heterobimetallic AuRu complex, consisting of a chloridogold(I) unit linked to a dichlorido(*p*-cymene)ruthenium(II) fragment via 1,4-bis(diphenylphosphino)butane, demonstrated a structural integrity in solution and solid state while undergoing controlled hydrolytic reactivity in aqueous medium. Aquatation occurred at rates comparable to related Ru(II) species, yet spectroscopic evidence confirmed that the Ru–µ-dppb–Au

bridge remained intact. Interaction with bovine serum albumin was moderate, with static fluorescence quenching and non-radiative energy transfer.

In vivo toxicological evaluation in Wistar rats revealed a favorable hepatic and renal safety profile. AST and ALT levels stayed within physiological limits, liver histology showed only mild and reversible changes, and kidney function markers (urea, creatinine) were unaffected despite sporadic structural alterations. On the other hand, hematological assays showed significant leukopenia and lymphopenia, accompanied by granulocytopenia, pointing toward immunomodulatory potential, while erythrocyte and platelet parameters remained largely preserved. Additional biochemical markers (LDH, CK) indicated reduced tissue injury compared to untreated animals.

The reported AuRu complex exhibits a combination of structural stability, controlled hydrolytic lability, and low hepatic or renal liabilities, while exerting measurable effects on immune cell populations. These results support this heterobimetallic platform for further mechanistic and therapeutic investigations, particularly in the context of anticancer drug development.

Supplementary Materials: The following supporting information can be downloaded at: https://www.mdpi.com/article/10.3390/inorganics13100323/s1. Crystallographic data for the AuRu complex have been deposited at the Cambridge Crystallographic Data Centre (CCDC) under deposition number CCDC 2481172 and can be obtained from https://www.ccdc.cam.ac.uk/structures or by emailing data_request@ccdc.cam.ac.uk. Electronic supplementary information (ESI) associated with this article is freely available online.

Author Contributions: Conceptualization, A.Z.; Methodology, A.Z., M.F. and A.V.; Investigation, A.Z., S.F., M.F., S.R., D.S., V.M., A.T., M.M.-B., I.O. and A.V.; Resources, A.Z.; Writing—Original Draft Preparation, A.Z., S.F., M.F., S.R., D.S. and V.M.; Writing—Review and Editing, A.Z., D.C.C. and A.V.; Visualization, A.Z., S.F., M.F., S.R. and V.M.; Supervision, A.Z. and A.V.; Project Administration, A.Z.; Funding Acquisition, A.Z. and I.O. All authors have read and agreed to the published version of the manuscript.

Funding: This work was supported by the Ministry of Science, Higher Education, and Youth of the Canton of Sarajevo through the RAES project (grant no. 27-02-35-33086-1/24, I.O.).

Institutional Review Board Statement: The study was approved by the Institutional Ethical Committee (Approval No. 01/01-3026/2-2024). All animals were housed under conventional conditions and handled in accordance with standard guidelines for the care and use of experimental animals, following established SOPs.

Informed Consent Statement: Not applicable.

Data Availability Statement: The original contributions presented in the study are included in the article/Supplementary Materials, further inquiries can be directed to the corresponding author.

Conflicts of Interest: The authors declare that they have no known competing financial interests or personal relationships that could have appeared to influence the work reported in this paper.

References

1. Khan, R.A.; Asim, A.; Kakkar, R.; Gupta, D.; Bagchi, V.; Arjmand, F.; Tabassum, S. A chloro-bridged heterobimetallic (η6-Arene) ruthenium–organotin complex as an efficient topoisomerase Iα inhibitor. *Organometallics* **2013**, *32*, 2546–2551. [CrossRef]
2. Massai, L.; Fernández-Gallardo, J.; Guerri, A.; Arcangeli, A.; Pillozzi, S.; Contel, M.; Messori, L. Design, synthesis and characterisation of new chimeric ruthenium (II)–gold (I) complexes as improved cytotoxic agents. *Dalton Trans.* **2015**, *44*, 11067–11076. [PubMed]
3. Wenzel, M.; Bigaeva, E.; Richard, P.; Le Gendre, P.; Picquet, M.; Casini, A.; Bodio, E. New heteronuclear gold (I)–platinum (II) complexes with cytotoxic properties: Are two metals better than one? *J. Inorg. Biochem.* **2014**, *141*, 10–16. [CrossRef] [PubMed]
4. Dougan, S.J.; Sadler, P.J. The design of organometallic ruthenium arene anticancer agents. *Chimia* **2007**, *61*, 704. [CrossRef]

5. Dyson, P.J. Systematic design of a targeted organometallic antitumour drug in pre-clinical development. *Chimia* **2007**, *61*, 698. [CrossRef]
6. Ronconi, L.; Sadler, P.J. Using coordination chemistry to design new medicines. *Coord. Chem. Rev.* **2007**, *251*, 1633–1648. [CrossRef]
7. Süss-Fink, G. Arene ruthenium complexes as anticancer agents. *Dalton Trans.* **2010**, *39*, 1673–1688.
8. Allardyce, C.S.; Dyson, P.J.; Ellis, D.J.; Heath, S.L. [Ru (η6-p-cymene) Cl2 (pta)](pta= 1, 3, 5-triaza-7-phosphatricyclo-[3.3. 1.1] decane): A water soluble compound that exhibits pH dependent DNA binding providing selectivity for diseased cells. *Chem. Commun.* **2001**, *15*, 1396–1397. [CrossRef]
9. Scolaro, C.; Bergamo, A.; Brescacin, L.; Delfino, R.; Cocchietto, M.; Laurenczy, G.; Geldbach, T.J.; Sava, G.; Dyson, P.J. In vitro and in vivo evaluation of ruthenium (II)− arene PTA complexes. *J. Med. Chem.* **2005**, *48*, 4161–4171. [CrossRef]
10. Allardyce, C.S.; Dyson, P.J.; Ellis, D.J.; Salter, P.A.; Scopelliti, R. Synthesis and characterisation of some water soluble ruthenium (II)–arene complexes and an investigation of their antibiotic and antiviral properties. *J. Organomet. Chem.* **2003**, *668*, 35–42.
11. Renfrew, A.K.; Phillips, A.D.; Egger, A.E.; Hartinger, C.G.; Bosquain, S.S.; Nazarov, A.A.; Keppler, B.K.; Gonsalvi, L.; Peruzzini, M.; Dyson, P.J. Influence of Structural Variation on the Anticancer Activity of RAPTA-Type Complexes: Ptn versus pta. *Organometallics* **2009**, *28*, 1165–1172. [CrossRef]
12. Vock, C.A.; Scolaro, C.; Phillips, A.D.; Scopelliti, R.; Sava, G.; Dyson, P.J. Synthesis, characterization, and in vitro evaluation of novel ruthenium (II) η6-arene imidazole complexes. *J. Med. Chem.* **2006**, *49*, 5552–5561. [CrossRef]
13. Morris, R.E.; Aird, R.E.; del Socorro Murdoch, P.; Chen, H.; Cummings, J.; Hughes, N.D.; Parsons, S.; Parkin, A.; Boyd, G.; Jodrell, D.I. Inhibition of cancer cell growth by ruthenium (II) arene complexes. *J. Med. Chem.* **2001**, *44*, 3616–3621. [CrossRef]
14. Habtemariam, A.; Melchart, M.; Fernández, R.; Parsons, S.; Oswald, I.D.; Parkin, A.; Fabbiani, F.P.; Davidson, J.E.; Dawson, A.; Aird, R.E. Structure—Activity relationships for cytotoxic ruthenium (II) arene complexes containing N, N-, N, O-, and O, O-chelating ligands. *J. Med. Chem.* **2006**, *49*, 6858–6868. [CrossRef]
15. Schmid, W.F.; John, R.O.; Arion, V.B.; Jakupec, M.A.; Keppler, B.K. Highly antiproliferative ruthenium (II) and osmium (II) arene complexes with paullone-derived ligands. *Organometallics* **2007**, *26*, 6643–6652. [CrossRef]
16. Ott, I. On the medicinal chemistry of gold complexes as anticancer drugs. *Coord. Chem. Rev.* **2009**, *253*, 1670–1681. [CrossRef]
17. Bindoli, A.; Rigobello, M.P.; Scutari, G.; Gabbiani, C.; Casini, A.; Messori, L. Thioredoxin reductase: A target for gold compounds acting as potential anticancer drugs. *Coord. Chem. Rev.* **2009**, *253*, 1692–1707. [CrossRef]
18. Carlos Lima, J.; Rodriguez, L. Phosphine-gold (I) compounds as anticancer agents: General description and mechanisms of action. *Anti-Cancer Agents Med. Chem. Anti-Cancer Agents* **2011**, *11*, 921–928. [CrossRef] [PubMed]
19. Hickey, J.L.; Ruhayel, R.A.; Barnard, P.J.; Baker, M.V.; Berners-Price, S.J.; Filipovska, A. Mitochondria-targeted chemotherapeutics: The rational design of gold (I) N-heterocyclic carbene complexes that are selectively toxic to cancer cells and target protein selenols in preference to thiols. *J. Am. Chem. Soc.* **2008**, *130*, 12570–12571. [CrossRef] [PubMed]
20. Oehninger, L.; Rubbiani, R.; Ott, I. N-Heterocyclic carbene metal complexes in medicinal chemistry. *Dalton Trans.* **2013**, *42*, 3269–3284. [CrossRef]
21. Kamei, H.; Koide, T.; Kojima, T.; Hashimoto, Y.; Hasegawa, M. Effect of gold on survival of tumor-bearing mice. *Cancer Biother. Radiopharm.* **1998**, *13*, 403–406. [CrossRef]
22. Stallings-Mann, M.; Jamieson, L.; Regala, R.P.; Weems, C.; Murray, N.R.; Fields, A.P. A novel small-molecule inhibitor of protein kinase Cι blocks transformed growth of non–small-cell lung cancer cells. *Cancer Res.* **2006**, *66*, 1767–1774. [CrossRef]
23. Meyer, A.; Bagowski, C.P.; Kokoschka, M.; Stefanopoulou, M.; Alborzinia, H.; Can, S.; Vlecken, D.H.; Sheldrick, W.S.; Wölfl, S.; Ott, I. On the biological properties of alkynyl phosphine gold (I) complexes. *Angew. Chem. Int. Ed.* **2012**, *51*, 8895. [CrossRef] [PubMed]
24. Chui, C.-H.; Wong, R.S.-M.; Gambari, R.; Cheng, G.Y.-M.; Yuen, M.C.-W.; Chan, K.-W.; Tong, S.-W.; Lau, F.-Y.; Bo-San Lai, P.; Lam, K.-H. Antitumor activity of diethynylfluorene derivatives of gold (I). *Bioorganic Med. Chem.* **2009**, *17*, 7872–7877. [CrossRef] [PubMed]
25. Yan, K.; Lok, C.-N.; Bierla, K.; Che, C.-M. Gold (I) complex of N, N′-disubstituted cyclic thiourea with in vitro and in vivo anticancer properties—Potent tight-binding inhibition of thioredoxin reductase. *Chem. Commun.* **2010**, *46*, 7691–7693. [CrossRef] [PubMed]
26. Köster, S.D.; Alborzinia, H.; Can, S.; Kitanovic, I.; Wölfl, S.; Rubbiani, R.; Ott, I.; Riesterer, P.; Prokop, A.; Merz, K. A spontaneous gold (I)-azide alkyne cycloaddition reaction yields gold-peptide bioconjugates which overcome cisplatin resistance in a p53-mutant cancer cell line. *Chem. Sci.* **2012**, *3*, 2062–2072. [CrossRef]
27. Simon, T.M.; Kunishima, D.H.; Vibert, G.J.; Lorber, A. Screening trial with the coordinated gold compound auranofin using mouse lymphocytic leukemia P388. *Cancer Res.* **1981**, *41*, 94–97.
28. Murray, B.S.; Babak, M.V.; Hartinger, C.G.; Dyson, P.J. The development of RAPTA compounds for the treatment of tumors. *Coord. Chem. Rev.* **2016**, *306*, 86–114. [CrossRef]
29. Madeira, J.; Gibson, D.; Kean, W.; Klegeris, A. The biological activity of auranofin: Implications for novel treatment of diseases. *Inflammopharmacology* **2012**, *20*, 297–306. [CrossRef]

30. Bertrand, B.; Citta, A.; Franken, I.L.; Picquet, M.; Folda, A.; Scalcon, V.; Rigobello, M.P.; Le Gendre, P.; Casini, A.; Bodio, E. Gold (I) NHC-based homo-and heterobimetallic complexes: Synthesis, characterization and evaluation as potential anticancer agents. *JBIC J. Biol. Inorg. Chem.* **2015**, *20*, 1005–1020. [CrossRef]
31. Elie, B.T.; Pechenyy, Y.; Uddin, F.; Contel, M. A heterometallic ruthenium–gold complex displays antiproliferative, antimigratory, and antiangiogenic properties and inhibits metastasis and angiogenesis-associated proteases in renal cancer. *JBIC J. Biol. Inorg. Chem.* **2018**, *23*, 399–411. [CrossRef]
32. Fernández-Gallardo, J.; Elie, B.T.; Sanaú, M.; Contel, M. Versatile synthesis of cationic N-heterocyclic carbene–gold (I) complexes containing a second ancillary ligand. Design of heterobimetallic ruthenium–gold anticancer agents. *Chem. Commun.* **2016**, *52*, 3155–3158. [CrossRef] [PubMed]
33. Batchelor, L.K.; Ortiz, D.; Dyson, P.J. Histidine targeting Heterobimetallic ruthenium (II)–gold (I) complexes. *Inorg. Chem.* **2019**, *58*, 2501–2513. [CrossRef] [PubMed]
34. Zahirović, A.; Roca, S.; Fočak, M.; Fetahović, S.; Višnjevac, A.; Topčagić, A.; Suljević, D.; Mitrašinović-Brulić, M.; Ostojić, J.; Muzika, V. Heterobinuclearity vs. Homobinuclearity in Ruthenium (II) and Gold (I) Organometallics with Diphosphine Ligands: Synthesis, Characterization, BSA Binding, and In Vivo Toxicity. In Proceedings of the 5th International Congress of Chemists and Chemical Engineers of Bosnia and Herzegovina, Sarajevo, Bosnia and Herzegovina, 27–30 June 2024; Book of Abstracts. p. 128.
35. Yang, Y.; Abboud, K.A.; McElwee-White, L. Heterobimetallic complexes with dppm-bridged Ru/Pd, Ru/Pt, Ru/Au and Ru/Cu centers. *Dalton Trans.* **2003**, *22*, 4288–4296. [CrossRef]
36. Maidich, L.; Zuri, G.; Stoccoro, S.; Cinellu, M.A.; Zucca, A. Assembly of symmetrical and unsymmetrical platinum (II) rollover complexes with bidentate phosphine ligands. *Dalton Trans.* **2014**, *43*, 14806–14815. [CrossRef]
37. Hancock, R.D. Chelate ring size and metal ion selection. The basis of selectivity for metal ions in open-chain ligands and macrocycles. *J. Chem. Educ.* **1992**, *69*, 615. [CrossRef]
38. Zahirović, A.; Fetahović, S.; Feizi-Dehnayebi, M.; Višnjevac, A.; Bešta-Gajević, R.; Kozarić, A.; Martić, L.; Topčagić, A.; Roca, S. Dual Antimicrobial-Anticancer Potential, Hydrolysis, and DNA/BSA binding affinity of a novel Water-Soluble Ruthenium-Arene ethylenediamine Schiff base (RAES) organometallic. *Spectrochim. Acta Part A Mol. Biomol. Spectrosc.* **2024**, *318*, 124528. [CrossRef]
39. Zahirović, A.; Roca, S.; Kahrović, E.; Višnjevac, A. Low DNA and high BSA binding affinity of cationic ruthenium (II) organometallic featuring pyridine and 2′-hydroxychalcone ligands. *J. Mol. Struct.* **2021**, *1236*, 130326. [CrossRef]
40. Zahirović, A.; Roca, S.; Višnjevac, A.; Kahrović, E. Ruthenium organometallics of chloro-substituted 2′-hydroxychalcones–A story of catecholase biomimetics beyond copper. *J. Organomet. Chem.* **2021**, *945*, 121863. [CrossRef]
41. Scolaro, C.; Hartinger, C.G.; Allardyce, C.S.; Keppler, B.K.; Dyson, P.J. Hydrolysis study of the bifunctional antitumour compound RAPTA-C, [Ru (η6-p-cymene) Cl2 (pta)]. *J. Inorg. Biochem.* **2008**, *102*, 1743–1748. [CrossRef]
42. Wang, F.; Chen, H.; Parsons, S.; Oswald, I.D.; Davidson, J.E.; Sadler, P.J. Kinetics of Aquation and Anation of Ruthenium (II) Arene Anticancer Complexes, Acidity and X-ray Structures of Aqua Adducts. *Chem. A Eur. J.* **2003**, *9*, 5810–5820. [CrossRef] [PubMed]
43. Topală, T.; Bodoki, A.; Oprean, L.; Oprean, R. Bovine serum albumin interactions with metal complexes. *Clujul Med.* **2014**, *87*, 215. [CrossRef]
44. Yamasaki, K.; Chuang, V.T.G.; Maruyama, T.; Otagiri, M. Albumin–drug interaction and its clinical implication. *Biochim. Biophys. Acta (BBA) Gen. Subj.* **2013**, *1830*, 5435–5443. [CrossRef]
45. Zahirović, A.; Žilić, D.; Pavelić, S.K.; Hukić, M.; Muratović, S.; Harej, A.; Kahrović, E. Type of complex–BSA binding forces affected by different coordination modes of alliin in novel water-soluble ruthenium complexes. *New J. Chem.* **2019**, *43*, 5791–5804. [CrossRef]
46. Coffer, M.T.; Shaw, C.F., III; Eidsness, M.; Watkins, J.; Elder, R. Reactions of auranofin and chloro (triethylphosphine) gold with bovine serum albumin. *Inorg. Chem.* **1986**, *25*, 333–339. [CrossRef]
47. Pratesi, A.; Cirri, D.; Ciofi, L.; Messori, L. Reactions of auranofin and its pseudohalide derivatives with serum albumin investigated through ESI-Q-TOF MS. *Inorg. Chem.* **2018**, *57*, 10507–10510. [CrossRef]
48. Hacker, R.M.; Smith, J.J.; Platt, D.C.; Brennessel, W.W.; Jones, M.A.; Webb, M.I. Ruthenium (II)–Arene Complexes with a 2, 2′-Bipyridine Ligand as Anti-Aβ Agents. *Biomolecules* **2025**, *15*, 475. [CrossRef]
49. Badr, H.E.; Elsayed, S.A.; Kawde, A.-N.; El-Hendawy, A.M. Development of Piano-Stool ruthenium (II) complexes: Synthesis, characterization, DNA/BSA binding affinity, in vitro cytotoxic and wound healing activity. *Inorg. Chem. Commun.* **2025**, *181*, 115287. [CrossRef]
50. Dömötör, O.; Enyedy, É.A. Binding mechanisms of half-sandwich Rh (III) and Ru (II) arene complexes on human serum albumin: A comparative study. *JBIC J. Biol. Inorg. Chem.* **2019**, *24*, 703–719. [CrossRef] [PubMed]
51. Bhuin, S.; Halder, S.; Saha, S.K.; Chakravarty, M. Binding interactions and FRET between bovine serum albumin and various phenothiazine-/anthracene-based dyes: A structure–property relationship. *RSC Adv.* **2021**, *11*, 1679–1693. [CrossRef]
52. Zahirović, A.; Tüzün, B.; Hadžalić, S.; Osmanković, I.; Roca, S.; Begić, S.; Fočak, M. Moderate DNA and high SARS-CoV-2 spike protein affinity of oxidovanadium (IV) complexes of 2-furoic acid hydrazones: In silico and in vitro approach. *J. Mol. Struct.* **2023**, *1294*, 136564. [CrossRef]

53. Yinhua, D.; Foroughi, M.M.; Aramesh-Boroujeni, Z.; Jahani, S.; Peydayesh, M.; Borhani, F.; Khatami, M.; Rohani, M.; Dusek, M.; Eigner, V. The synthesis, characterization, DNA/BSA/HSA interactions, molecular modeling, antibacterial properties, and in vitro cytotoxic activities of novel parent and niosome nano-encapsulated Ho (III) complexes. *RSC Adv.* **2020**, *10*, 22891–22908. [CrossRef] [PubMed]
54. Ahmed, A.; Alkhawajah, A.M.M.; Al-Tamimi, D.M.; Shawarby, M.A.; Isab, A.A.; Badar, A. Biological alterations in renal and hepatic tissues by a novel gold (III) anti-cancerous compound. *Iran. J. Basic Med. Sci.* **2018**, *21*, 1064.
55. Mabuza, L.P.; Gamede, M.W.; Maikoo, S.; Booysen, I.N.; Ngubane, P.S.; Khathi, A. Effects of a ruthenium schiff base complex on glucose homeostasis in diet-induced pre-diabetic rats. *Molecules* **2018**, *23*, 1721. [CrossRef]
56. Hou, S.-M.; Hsia, C.-H.; Velusamy, M.; Jayakumar, T.; Hsia, C.-W.; Chang, C.-C.; Lin, K.-H.; Lu, Y.-C. Ruthenium complex, TQ-5, protects against LPS-induced macrophage inflammation and acute liver injury in mice via downregulating NF-κB pathways. *Int. J. Mol. Med.* **2019**, *44*, 335–345. [CrossRef] [PubMed]
57. Manibusan, M.K.; Odin, M.; Eastmond, D.A. Postulated carbon tetrachloride mode of action: A review. *J. Environ. Sci. Health Part C* **2007**, *25*, 185–209. [CrossRef] [PubMed]
58. Ciftci, O.; Beytur, A.; Vardi, N.; Ozdemir, I. Evaluation of reproductive toxicity in male rats treated with novel synthesized ruthenium (II) and gold (I)-NHC complexes. *Drug Dev. Ind. Pharm.* **2012**, *38*, 40–46. [CrossRef]
59. Yue, S.; Luo, M.; Liu, H.; Wei, S. Recent advances of gold compounds in anticancer immunity. *Front. Chem.* **2020**, *8*, 543. [CrossRef]
60. Rinaldi-Neto, F.; Ribeiro, A.B.; Ferreira, N.H.; Squarisi, I.S.; Oliveira, K.M.; Orenha, R.P.; Parreira, R.L.T.; Batista, A.A.; Tavares, D.C. Anti-melanoma effect of ruthenium (II)-diphosphine complexes containing naphthoquinone ligand. *J. Inorg. Biochem.* **2021**, *222*, 111497. [CrossRef]
61. Nobili, S.; Mini, E.; Landini, I.; Gabbiani, C.; Casini, A.; Messori, L. Gold compounds as anticancer agents: Chemistry, cellular pharmacology, and preclinical studies. *Med. Res. Rev.* **2010**, *30*, 550–580. [CrossRef]
62. Bertrand, B.; Casini, A. A golden future in medicinal inorganic chemistry: The promise of anticancer gold organometallic compounds. *Dalton Trans.* **2014**, *43*, 4209–4219. [CrossRef]
63. Zhang, L.; Wang, P.; Zhou, X.-Q.; Bretin, L.; Zeng, X.; Husiev, Y.; Polanco, E.A.; Zhao, G.; Wijaya, L.S.; Biver, T. Cyclic ruthenium-peptide conjugates as integrin-targeting phototherapeutic prodrugs for the treatment of brain tumors. *J. Am. Chem. Soc.* **2023**, *145*, 14963–14980. [CrossRef]
64. Bennett, M.; Huang, T.N.; Matheson, T.; Smith, A.; Ittel, S.; Nickerson, W. 16.(η6-Hexamethylbenzene) ruthenium complexes. *Inorg. Synth.* **1982**, *21*, 74–78.
65. Doherty, S.; Knight, J.G.; Rath, R.K.; Clegg, W.; Harrington, R.W.; Newman, C.R.; Campbell, R.; Amin, H. Ruthenium complexes of six-electron-donor NUPHOS-type diphosphines: Highly selective catalysts for the hydrocarboxylation of terminal alkynes. *Organometallics* **2005**, *24*, 2633–2644. [CrossRef]
66. Uson, R.; Laguna, A.; Laguna, M.; Briggs, D.; Murray, H.; Fackler, J., Jr. (Tetrahydrothiophene) gold (I) or gold (III) complexes. *Inorg. Synth.* **1989**, *26*, 85–91.
67. Berners-Price, S.J.; Sadler, P.J. Gold (I) complexes with bidentate tertiary phosphine ligands: Formation of annular vs. tetrahedral chelated complexes. *Inorg. Chem.* **1986**, *25*, 3822–3827. [CrossRef]
68. Zahirović, A.; Osmanković, I.; Turkušić, E.; Kahrović, E. Improved method for spectrophotometric determination of ruthenium using 1, 10-phenanthroline: Application for analysis of complex compounds. *Anal. Methods* **2018**, *10*, 5078–5083. [CrossRef]
69. Sheldrick, G.M. SHELXT–Integrated space-group and crystal-structure determination. *Acta Crystallogr. Sect. A Found. Adv.* **2015**, *71*, 3–8. [CrossRef] [PubMed]
70. Sheldrick, G.M. Crystal structure refinement with SHELXL. *Acta Crystallogr. Sect. C Struct. Chem.* **2015**, *71*, 3–8. [CrossRef]
71. Macrae, C.F.; Bruno, I.J.; Chisholm, J.A.; Edgington, P.R.; McCabe, P.; Pidcock, E.; Rodriguez-Monge, L.; Taylor, R.; Streek, J.; Wood, P.A. Mercury CSD 2.0–new features for the visualization and investigation of crystal structures. *J. Appl. Crystallogr.* **2008**, *41*, 466–470. [CrossRef]
72. Spek, A.L. Structure validation in chemical crystallography. *Acta Crystallogr. Sect. D Biol. Crystallogr.* **2009**, *65*, 148–155. [CrossRef]
73. Farrugia, L.J. WinGX suite for small-molecule single-crystal crystallography. *J. Appl. Crystallogr.* **1999**, *32*, 837–838. [CrossRef]
74. da Silva, M.M.; Ribeiro, G.H.; de Camargo, M.S.; Ferreira, A.G.; Ribeiro, L.; Barbosa, M.I.; Deflon, V.M.; Castelli, S.; Desideri, A.; Correa, R.S. Ruthenium (II) diphosphine complexes with mercapto ligands that inhibit topoisomerase IB and suppress tumor growth in vivo. *Inorg. Chem.* **2021**, *60*, 14174–14189. [CrossRef]
75. Mahmud, K.M.; Niloy, M.S.; Shakil, M.S.; Islam, M.A. Ruthenium complexes: An alternative to platinum drugs in colorectal cancer treatment. *Pharmaceutics* **2021**, *13*, 1295. [CrossRef] [PubMed]
76. Mello-Andrade, F.; Cardoso, C.G.; e Silva, C.R.; Chen-Chen, L.; de Melo-Reis, P.R.; de Lima, A.P.; Oliveira, R.; Ferraz, I.B.M.; Grisolia, C.K.; Almeida, M.A.P. Acute toxic effects of ruthenium (II)/amino acid/diphosphine complexes on Swiss mice and zebrafish embryos. *Biomed. Pharmacother.* **2018**, *107*, 1082–1092. [CrossRef]

77. Mihajlovic, K.; Milosavljevic, I.; Jeremic, J.; Savic, M.; Sretenovic, J.; Srejovic, I.; Zivkovic, V.; Jovicic, N.; Paunovic, M.; Bolevich, S. Redox and apoptotic potential of novel ruthenium complexes in rat blood and heart. *Can. J. Physiol. Pharmacol.* **2021**, *99*, 207–217. [CrossRef] [PubMed]
78. Suljevic, D.; Focak, M.; Filipic, F.; Hamzic, A.; Zubcevic, N.; Alijagic, A. Haematopoiesis in the European common toad Bufo bufo (Linnaeus, 1758): New methodological insights to study general, seasonal, and sexual haematopoietic distribution and maturation pattern. *Turk. J. Zool.* **2018**, *42*, 198–206. [CrossRef]

Disclaimer/Publisher's Note: The statements, opinions and data contained in all publications are solely those of the individual author(s) and contributor(s) and not of MDPI and/or the editor(s). MDPI and/or the editor(s) disclaim responsibility for any injury to people or property resulting from any ideas, methods, instructions or products referred to in the content.